DOI:
10.1021/acs.nanolett.6b03203

Document Version
Peer reviewed version

Promoting atoms into delocalized long-living magnetically modified state using Atomic Force Microscopy

Y. Kinoshita,[†] R. Turanský,[‡] J. Brndiar,[‡] Y. Naitoh,[†] Y. J. Li,[†] L. Kantorovich,[¶] Y. Sugawara,[†] and I. Štich[*,‡,§]

† *Dept. of Applied Physics, Osaka University, Japan*
‡ *Inst. of Physics, CCMS, Slovak Academy of Sciences, Bratislava, Slovakia*
¶ *Dept. of Physics, King's College London, U.K.*
§ *Ruprecht A. Institute of Technology, Bratislava, Slovakia*

E-mail: ivan.stich@savba.sk

Abstract

We report on a low-temperature AFM manipulation of Co atoms in UHV on an oxidized copper surface in which the manipulated atom is kept delocalized above several surface unit cells over macroscopic times. The manipulation employed, in addition to the ubiquitous short-range tip-generated chemical forces, also long-range forces generated via Friedel oscillations of the metal charge density due to Co nanostructures prearranged on the surface by lateral manipulation. We show that our manipulation protocol requires mechanical control of the spin state of the Co atom.

Keywords: AFM manipulation, magnetic atoms, mechanical control of spin, Friedel oscillations.

Scanning probe microscopies (SPM), such as scanning tunneling microscopy (STM) and non-contact atomic force microscopy (NC-AFM), have played a key role in constructing nanostructures with atomic dimensions. STM and NC-AFM have a number of unique abilities such as scanning surfaces with atomic resolution,[1] providing information on the chemical identity of the scanned atoms,[2] and perhaps the most fascinating ability of performing nano-manipulations.[3–5] Both lateral[6,7] and vertical[8–10] atomic manipulations have been performed to build bottom-up nanostructures on surfaces either by moving the manipulated atoms directly[6,11] or by exchanging pairs of atoms.[9,12] All these manipulations have been performed with non-magnetic atoms on high-symmetry (111) and (001) substrates and have strongly relied on short-range site-specific chemical interactions.[4] Here we show that by harnessing both short- ($\leq$5Å) and long-range ($\approx$ 5 - 40 Å) interactions exerted on magnetic atoms, novel manipulation protocols can be designed whereby in a controlled way the manipulated atoms can be kept in a magnetically modified state which is imaged over macroscopic times as delocalized above several surface unit cells.

Friedel oscillations[13,14] of metal surface charge density due to adatoms or adatom superstructures adsorbed on it may provide a natural mechanism of long-range interaction forces exerted on an adatom which is manipulated by an SPM tip. However, combining these rather weak (in the range of meV [13,14]) interactions with the short range chemical interaction of the adatom with the substrate (and possibly the tip) is challenging as the latter interaction is rather strong (typically in the eV range). Existence of strong short-range

forces is essential in trapping the adatoms in the desired positions when building nanostructures, as otherwise they would be undesirably highly mobile at finite temperatures and be easily moved by the tip. However, as will be demonstrated here, if the short-range interaction provides a highly corrugated potential energy surface (PES), which contains smooth plateaus separated by deep minima, then the long-range interaction due to the surrounding adatoms provided by the Friedel oscillations, may have profound implications on the manipulated adatom.

One example of such a system with the required form of the PES is a cobalt adatom adsorbed on the $p(2 \times 1)$ phase of the oxidized Cu(110) surface ($p(2 \times 1)$Cu(110):O). The $p(2 \times 1)$ surface shown in Fig. 1 has an alternating row/missing row conformation[18,19] in the $[1\bar{1}0]$ direction, while along the [001] lie alternating rows of Cu and O atoms.

All experiments were carried out with a home-built NC-AFM operating under ultrahigh vacuum condition at 78 K. Manipulation experiments were performed by decreasing Δf by -2 Hz before a manipulation was attempted and switching back to the imaging mode afterwards. We have performed two types of manipulation. While the standard lateral manipulation has an activation barrier of ≈1 eV, the novel delocalization manipulation has a barrier twice as large (see below). Therefore we have been able to perform only a handful of such manipulations and discuss here the most illustrative ones. More experimental details can be found in supporting information (SI).

A large-scale NC-AFM image of a $p(2 \times 1)$ terrace is shown in the right panel of Fig. 1. From the image of the $c(6 \times 2)$ phase, seen at the bottom of the figure, we can safely conclude that both imaging and manipulation have been performed with an O-terminated tip,[21,22] which remained stable over many hours. The O-terminated tip images Cu atoms as bright spots,[22] clearly visible in Fig. 1. The brightest spots in Fig. 1 are Co atoms which appear to adsorb preferentially in the between-O bonded positions along the $[1\bar{1}0]$ direction (between two neighboring Cu-O rows). The Co atoms in the

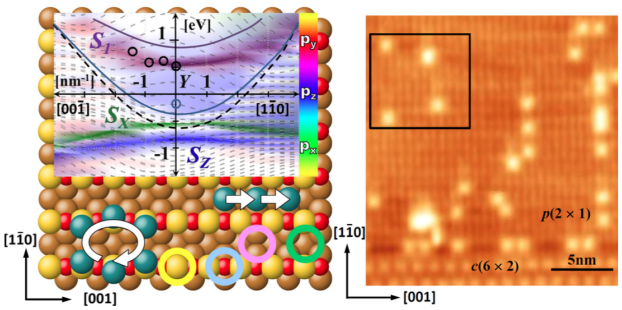

Figure 1: **Left panel**: Ball model of the $p(2 \times 1)$Cu(110):O surface, where red, yellow, and brown balls depict O, added Cu, and bulk Cu atoms, respectively. The on-top-Cu, on-top-O, between-Cu, and between-O positions are indicated by yellow, blue, green, and pink circles, respectively. The Co atoms, depicted in green, highlight the delocalization and lateral manipulations, see the text. The inset shows the calculated band structure around the **Y**-point in the Brillouin zone, see the SI, of the $p(2 \times 1)$Cu(110):O surface projected onto p-orbitals of the oxygen-copper row. Shown from the top to the bottom are the unoccupied S_1 surface state (p_z on Cu, p_y on O) at ≈+0.5 eV along with photoemission spectra[15] (black empty circles), the broad satellite (p_z on O) delimited from above by violet and from below by blue parabolas, experimentally detectable as a broad feature at ≈-0.2 eV[16] (blue empty circle), and two strong antibonding surface states S_x (p_x)/S_z (p_z) strongly localized on the oxygen atoms at ≈-0.6/-0.8 eV clearly detectable experimentally.[16] The lower border of the projected bulk band gap is shown by black dashed line, the upper border, not shown, is around 4 eV above it. **Right panel**: Large-scale topographic image showing Co atoms deposited on the $p(2 \times 1)$ terrace. At the bottom of the image a stripe of the $c(6 \times 2)$ phase is seen. The square box shows the manipulation area with four Co atoms prearranged at suitable positions some distance away from each other.

square box in Fig. 1 have been prearranged in positions deemed suitable for demonstrating the peculiar manipulation mechanism as discussed below.

The atomic rearrangements in the manipulation area are shown in Figs. 2(a - f). The

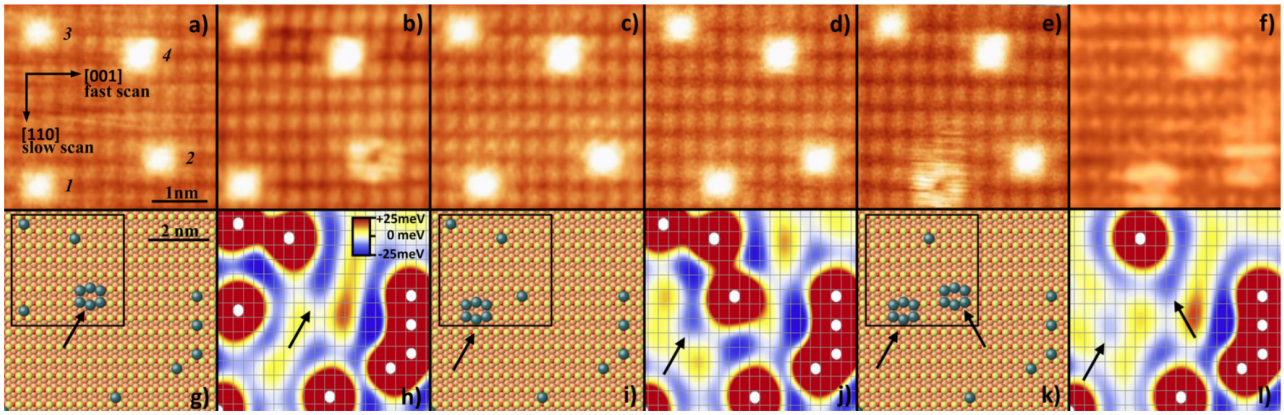

Figure 2: NC-AFM manipulation of Co atoms labeled *1* - *4* in panel (a). (a) - (f) sequence of images taken in chronological order, but not necessarily one after the other, showing the delocalization manipulation, (b), (e), and (f) of atoms *2*, *1*, and of both *1* and *2*, respectively, and an ordinary lateral manipulation of atom *1* successively by two lattice parameters, (c) and (d). In (f) extraction of atom *3* by vertical manipulation is also seen. (g), (i), and (k) show three large-scale models of the delocalization processes from panels (b), (e), (f) and the corresponding Friedel PESs, U_{mod} (truncated above +25 meV close to the atomic positions), in (h), (j) and (l), calculated with 11 Co atoms in the range of ≈40 Å from the actual position of the manipulation event. An elliptical Fermi edge is assumed when applying Eq. (2) to predict the azimuthal dependence of the Friedel interaction[17] using $m^{\star}_{[001]} = 0.44\ m_e$, $m^{\star}_{[1\bar{1}0]} = 0.57\ m_e$, $E_0 = 0.2$ eV, and $\delta_0 \approx \pi/2$ as fitting parameters. Arrows indicate the delocalized Co atoms positions in the AFM images and the corresponding minima on the Friedel PESs. The grey grids correspond to positions of substrate Cu atoms in the AFM images. The Friedel PESs in the simple form outlined in panels h), j), l) are only valid at high symmetry points in the surface unit cell, i.e. in the on-top-Cu (grey grids), the between-oxygen, and the between-Cu sites, see SI.

four relevant Co atoms are numbered in Fig. 2(a). First a "*delocalization*" manipulation can be seen in Fig. 2(b), where Co atom *2* is found spontaneously delocalized over roughly six substrate Cu atoms, see schematics in Fig. 1. After that, a sequence of two consecutive *lateral manipulations* of Co atom *1* in the [001] direction is seen in Figs. 2(c, d), while the Co atom *2* becomes localized again. Another delocalization manipulation, this time of Co atom *1*, is seen in Fig. 2(e). Finally, extraction of atom *3* by a *vertical manipulation* shown in Fig. 2(f) is followed by the delocalization of atom *2* again, leaving now both atoms *1* and *2* in a delocalized state. While removal of atom *3* does not change the nature of the delocalization manipulation, as explained below, removal of one Co atom modifies the details of the PES for atom *1*. Importantly, as it follows from the observed images, the delocalization pattern remains stable over *macroscopic* times. The experimental life-time of the delocalization manipulation is ≈1 minute for atom *2* and in excess of 20 minutes for atom *1*. The differences in life-time of atoms *1*and *2* reflect the statistical nature of the manipulation process and/or the differences in surrounding Co atoms that create a different potential well around these two positions.

The lateral manipulations represent a fairly standard type of a manipulation customarily observed in the past.[6,7] The vertical manipulation appears similar to that observed on the $p(2 \times 1)$ surface for Cu atoms.[10] However, to the best of our knowledge, the observed delocalization of atoms over the regions comprised of the multiple substrate atoms, represents a *novel* type of manipulation induced, as we argue below, by the activation of the long-range forces in the manipulation process triggered by the Co atom spin change.

To rationalize the observed long-lived delocalized state of the Co atoms during their manip-

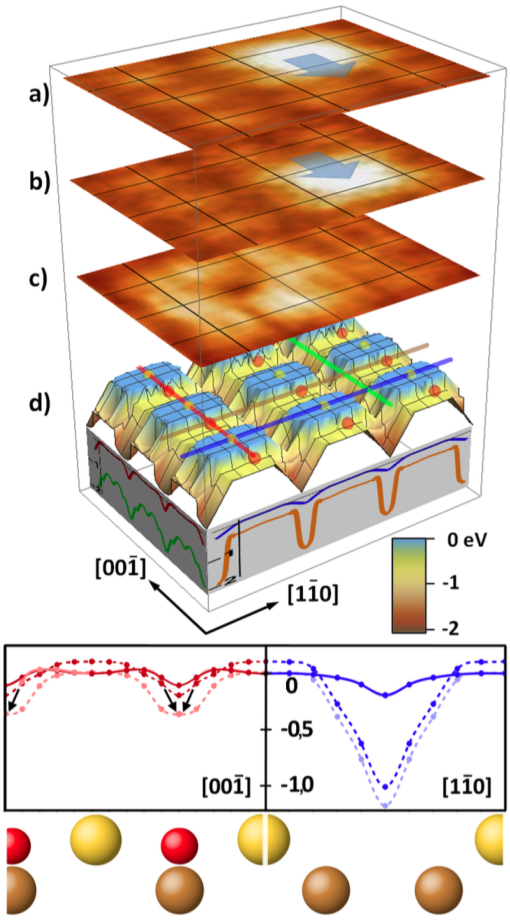

Figure 3: **Top panel:** Experimental images (a-c) of the atom lateral, from a) to b), and delocalization, c), manipulations, placed on top of the DFT calculated (U = 0) adiabatic PES, U_{sr}, d), of the Co atom in the [Ar]d^8 state on the $p(2 \times 1)$Cu(110):O surface. The circular character of the image of the Co atom in the delocalized state is clearly seen in c). **Bottom panel:** Detailed representation of PESs, in eV, along on-top-Cu – on-top-O – on-top-Cu ([001] direction, red lines) and on-top-Cu – between Cu – on-top-Cu ([1$\bar{1}$0] direction, blue lines) directions in [Ar]d^7 (full lines) and [Ar]d^8 (dashed lines) local Co spin configurations for U = 9 eV (dark color) and for U = 7 (light color). Note that the PESs in the [Ar]d^7 state for U = 9 eV and U = 7 eV are barely distinguishable on the scale of the figure (half shown in red and half in pink); the main difference being that the [Ar]d^7 configuration is unstable in the on-top-O position for U = 7 eV and transforms into [Ar]d^8 (depicted by arrows). For details see SI.

ulation, we performed extensive density functional theory (DFT) calculations for [Ar]d^7 and [Ar]d^8 Co configurations. A series of $U = 0$ eV calculations was run first for the entire PES which is shown in the upper panel of Fig. 3. Only the [Ar]d^8 Co configuration was found stable over the entire PES. The $U = 0$ eV calculations were followed by test calculations with $U \in$ (4-9) eV. The effect of U is to localize the d electrons spatially and thus make them less reactive. Increasing the value of U leads to a less corrugated PES with larger plateaus over the on-top-Cu positions; it does not, however, modify qualitatively the form of the PES as becomes clear from the potential energy curves calculated along two particular directions on the surface and shown in the lower panel of Fig. 3 (more details are in the SI).

The calculated adiabatic PES for a single Co atom over the $p(2 \times 1)$Cu(110):O surface is correlated with the manipulation processes observed experimentally, see Fig. 3. The PES of the [Ar]d^8 state depicts only the short-range part, U_{sr}, of the interaction potential acting on a Co atom due to the surface. The PES is highly unusual, featuring very large (≈2×3 Å^2) barely corrugated plateaus over added row Cu atoms (blue areas on the PES) connected by very shallow (0.1 - 0.2 eV) minima in the [001] direction along the Cu-O-Cu added row (red line) and [1$\bar{1}$0] direction (blue line) in-between-Cu atoms. On the contrary, the PES is highly corrugated (≈ 1 eV, brown areas) in-between (green line) and across (the brown line) the oxygen atoms where the absolute minima at the between-O bonded sites lie. Hence, while the between-O bonded sites are able to firmly anchor the Co atoms in [Ar]d^8 state, they can be laterally manipulated by the tip between these sites along the [001] direction, the process shown in Fig. 2(c, d).

The spin state of the delocalized Co atom is predicted to assume the less reactive atomic-like [Ar]d^7 configuration, Fig. 3. The delocalization manipulation, Figs. 2(b, e, f), requires first for the manipulated Co atom to assume an on-top-Cu atom position, which clearly means surmounting a large barrier of ∼2 eV and the [Ar]d^8 → [Ar]d^7 local spin modification. This

process is stochastic and has a fairly small probability. However, once the Co atom is promoted onto the plateau over the added row Cu atom, it accepts the lower energy [Ar]d^7 state, and then the tiny minima separating the plateaus (see the bottom panel in Fig. 3) can be easily bridged by the tip. Hence the atom may, with a high probability, remain in the weakly corrugated part of the PES for a long time at small enough temperatures. The flatness of the PES along the smeared out manipulation trajectory is supported also by the absence of a signal from the dissipation channel. Contrary, assuming that the Co atom retains its [Ar]d^8 ground-state spin configuration means that it would have to surmount a huge energy barrier of $\approx$ 1.2 eV, Fig. 3, on passing between the experimentally visited on-top-Cu positions via the between-Cu position, in clear disagreement with the manipulation images in Fig. 2. Note that by promoting Co atom into the metastable on-top-Cu [Ar]d^7 state, the NC-AFM tip effectively performs a *mechanical control* of the local *Co spin configuration*.

The potential U_{sr} in Fig. 3(d) predicts only manipulation of atoms along straight lines. In order for the trajectory to assume a smeared out circular path, as observed experimentally, an additional modulation potential, U_{mod}, is needed to localize the Co atom on the plateau. Since the manipulation was observed on several sites, U_{mod} could not be generated by surface defects. Also, it cannot be caused by the surface stress[28] induced by adsorbed Co atoms as it decays monotonically from them. We propose that U_{mod} is generated by the long-range interaction between the Co adatoms caused by Friedel charge density oscillations around them due to an effective surface state. Indeed, a $p(2 \times 1)$Cu(110):O photoemission spectrum shows an unoccupied parabolic surface state at around +0.4 eV[15,16] along the $[00\bar{1}]$ direction, S_1 in Fig. 1, and a broad occupied surface oxygen state at $\approx$-0.2 eV with respect to Fermi energy, S_s, see Fig. 1, forming effectively a satellite to the S_1 state. The S_1 state, with a similar dispersion along the $[1\bar{1}0]$ direction, was also found in DFT calculations.[20] However, to the best of our knowledge, the S_s feature has not been identified by DFT calculations as yet.

Our DFT calculations, see left panel of Fig. 1 and SI, show an occupied band of surface states on the pristine $p(2 \times 1)$ surface able to screen the interaction between Co atoms via the Friedel oscillation mechanism. These surface states are further lowered in energy by $\approx$0.15 eV upon adsorption of a Co atom, see SI. We approximate that band of states by an effective surface state S_{eff} with an asymmetric parabolic dispersion

$$E(\vec{k}) = \frac{\hbar^2 k_x^2}{2m^\star_{[001]}} + \frac{\hbar^2 k_y^2}{2m^\star_{[1\bar{1}0]}} - E_0 \ , \qquad (1)$$

with E_0 being the minimum energy offset.

In the simplest approximation the pairwise interaction between two adatoms placed relatively to each other by a vector $\vec{r}$ due to the Friedel oscillation mechanism is [13,14]

$$U_{mod}(\vec{r}) \propto \frac{\sin(2\vec{k_F} \cdot \vec{r} + 2\delta_0)}{(\vec{k_F} \cdot \vec{r})^2} \ , \qquad (2)$$

where k_F is the Fermi wave vector of the surface state electrons and δ_0 is the phase shift describing the scattering properties of the Co atom. For a generalization to an elliptical Fermi edge actually used in our modeling, see SI.

The plots in Figs. 2 (h, j, l) show $U_{mod}(\vec{r})$ simulated by summing up pair-wise contributions from all Co atoms within a circle of $\approx$40 Å radius taken around the Co atom(s) of interest, as shown in our images of the delocalization processes in Fig. 2 (b, e, f), respectively. Despite approximations made (pair-wise interactions, neglect of the structural relaxation upon Co atom adsorption, the fitting procedure) they indeed predict minima at positions corresponding to the delocalization pattern observed experimentally. All the minima of U_{mod} experimentally observed correspond to the first minima of the Friedel oscillating interaction generated mainly by atoms *1* - *4*, and azimuthally modulated by other atoms surrounding them. The only exception being the minimum corresponding to atom *1* in Fig 2 (l) which, due to removal of atom *3*, now features a much weaker second minimum. In this case, though, the

minimum is circularly surrounded by four maxima and hence forms a spatially well distinct entity. While relatively weak, the U_{mod} may still provide a restricting potential sufficient to constrain the Co atom on the plateau. Moreover, due to very small energy barriers within it (small corrugation of U_{sr}), the Co atom will be highly mobile there. This high mobility within a small lateral region is manifested itself in the circularly shaped smeared out NC-AFM images taken by a relatively slowly moving tip during the scan.

As evident from Fig. 2, the delocalization pattern may be controlled by specific pre-defined positions of the surrounding Co atoms, adjustable by ordinary lateral manipulation, that would provide the desirable long-range constraining potential U_{mod}, which, in general, need *not* limit the delocalization pattern to six substrate atoms, see also SI. In principle, the manipulated magnetic atom could be encapsulated into a "Friedel cage"and kept localized around the on-top-Cu position.

In summary, we have performed manipulation of Co atoms on a lower-symmetry substrate, the $p(2 \times 1)$Cu(110):O surface, under the combined action of short-range chemical forces induced by the tip of the microscope and the surface, and long-range forces induced via Friedel oscillations of charge density due to other adsorbates. We have observed a novel manipulation of Co atoms that could be kept, over macroscopic times, delocalized above several surface atoms. We demonstrate that the manipulation is possible due to the modification of the spin state of the manipulated atom, and hence we also demonstrate the possibility of mechanical control over the spin state of the atom as a result of the manipulation. This may be of importance for spintronics applications.[29] Similarly the $d^8 \leftrightarrow d^7$ "control"of the magnetic state of the Co atom on graphene was achieved by Ir(111) $\leftrightarrow$ Ru(0001) substrate modification.[30]

Methods. In our experiments the deflection of the cantilever was detected by optical interferometer. The frequency-modulation technique was used to detect the tip-sample interaction. Commercially available Si cantilevers (n-type, Nanoworld NCL, 40 Nm^{-1}, 150 kHz) were used. The tip apex was cleaned in situ by Ar ion bombardment at an energy of 0.6 keV. The frequency shift of the oscillating cantilever was measured by using phase-locked-loop-based commercial electronics (easyPLL plus detector and controller, Nanosurf, Liestal, Switzerland). The Cu(110):O surface was prepared by cleaning using repeated Ar ion sputtering and subsequently annealing at 550°C, followed by exposure of oxygen at 300°C. The set point of frequency shift was selected in the range of -30 Hz to -37 Hz. Weak low pass image filtering was used.

In our calculations the surface was modelled using a five layer Cu-slab with the upper three atomic layers allowed to relax.[21,22] Calculations of the energies and forces were performed using DFT with projector augmented-wave pseudopotentials[23] and 500 eV plane wave cut-off as implemented in the VASP code.[24] Since van der Waals interactions were found to be essential for the O-terminated Cu surfaces,[25] this interaction was accounted for here using the vdW-DF2 scheme.[26] The effect of electronic correlation of localized Co d electrons was taken into account by DFT+U method with U between 7 and 9 eV.[27] All calculations were performed in global spin quartet multiplicity. More simulation details can be found in SI.

Acknowledgement Work supported by the Grant-in-Aid for Scientific Research of Japan, by APVV-0207-11, VEGA (2/0007/12, 2/0162/15) projects. We also gratefully acknowledge use of the Hitachi SR16000/M1 supercomputer system at CCMS/IMR, Tohoku University, Japan.

Supporting Information Available: Further experimental and computational details, such as additional AFM images, computed short-range PESs, and discussion of generalization of the Friedel PESs for off-zone center surface states are summarized in SI. This material is available free of charge via the Internet at `http://pubs.acs.org/`.

References

(1) Binnig, G.; Rohrer, H.; Gerber, C.; Weibel, E. *Phys. Rev. Lett.* **1982**, *49*, 57.

(2) Sugimoto, Y.; P., P.; Abe, M.; Jelinek, P.; Perez, P.; Morita, S.; Custance, O. *Nature* **2007**, *446*, 64.

(3) Eigler, D. M.; Schweizer, E. K. *Nature* **1990**, *344*, 524.

(4) Custance, O.; Perez, R.; Morita, S. *Nature Nanotechnology* **2009**, *9*, 803.

(5) Sugimoto, Y.; Yurtsever, A.; Hirayama, N.; Abe, M.; Morita, S. *Nat. Commun.* **2014**, *5*, 4360.

(6) Sugimoto, Y.; Jelinek, P.; Pou, P.; Abe, M.; Morita, S.; Pérez, R.; Custance, O. *Phys. Rev. Lett.* **2007**, *98*, 106104.

(7) Ternes, M.; Lutz, C. P.; Hirjibehendin, C. F.; Giessible, F. J.; Heinrich, A. J. *Science* **2008**, *319*, 1066.

(8) Oyabu, N.; Custance, O.; Yi, I.; Sugawara, Y.; Morita, S. *Phys. Rev. Lett.* **2003**, *90*, 176102.

(9) Sugimoto, Y.; Pou, P.; Custance, O.; Jelinek, P.; Abe, M.; Pérez, R.; Morita, S. *Science* **2008**, *322*, 413.

(10) Bamidele, J.; Lee, S. H.; Kinoshita, Y.; Turanský, R.; Naitoh, Y.; Li, Y. J.; Sugawara, Y.; Štich,; Kantorovich, L. *Nat. Commun.* **2014**, *5*, 4476.

(11) Oyabu, N.; Sugimoto, Y.; Abe, M.; Custance, O.; Morita, S. *Nanotechnology* **2005**, *16*, S112.

(12) Sugimoto, Y.; Abe, M.; Hirayama, S.; Oyabu, N.; Custance, O.; Morita, S. *Nature Mater.* **2005**, *4*, 156.

(13) Hyldgaard, P.; Persson, M. *J. Phys.: Condens. Matter* **2000**, *12*, L13.

(14) Ternes, M.; Pivetta, M.; Patthey, F.; Schneider, W.-D. *Prog. Surf. Sci.* **2010**, *85*, 1.

(15) Jacob, W.; Dose, V.; Goldmann, A. *Appl. Phys. A* **1986**, *41*, 145.

(16) Courths, R.; Hüfner, S.; Kemkes, P.; Wiesen, G. *Surf. Sci.* **1997**, *376*, 43.

(17) Patrone, P. N.; Einstein, T. L. *Phys. Rev. B* **2012**, *85*, 045429.

(18) Ruan, L.; Besenbacher, F.; Stensgaard, I.; Laegsgaard, E. *Phys. Rev. Lett.* **1993**, *70*, 4079.

(19) Kishimoto, S.; Kageshima, M.; Naitoh, Y.; Li, Y. J.; Sugawara, Y. *Surf. Sci.* **2008**, *602*, 2175.

(20) Harl, J.; Kresse, G.; Sun, L. D.; Hohage, M.; Zeppenfeld, P. *Phys. Rev. B* **2007**, *76*, 035436.

(21) Bamidele, J.; Kinoshita, Y.; Turanský, R.; Lee, S. H.; Naitoh, Y.; Li, Y. J.; Sugawara, Y.; Štich, I.; Kantorovich, L. *Phys. Rev. B* **2012**, *86*, 155422.

(22) Bamidele, J.; Kinoshita, Y.; Turanský, R.; Lee, S. H.; Naitoh, Y.; Li, Y. J.; Sugawara, Y.; Štich, I.; Kantorovich, L. *Phys. Rev. B* **2014**, *90*, 035410.

(23) Blöchl, P. E. *Phys. Rev. B* **1994**, *50*, 17953.

(24) Kresse, G.; Furthmüller, J. *Comput. Mater. Sci.* **1996**, *6*, 15.

(25) Bamidele, J.; Brndiar, J.; Gulans, A.; Kantorovich, L.; Štich, I. *J. Chem. Theor. Comp.* **2013**, *20*, 5578.

(26) Lee, K.; Murray, E. D.; Kong, L.; Lundqvist, B. I.; Langreth, D. C. *Phys. Rev. B* **2010**, *82*, 081101.

(27) Anisimov, V. I.; Zaanen, J.; Andersen, O. K. *Phys. Rev. B* **1991**, *44*, 943.

(28) Whitman, L. J.; Strocio, J. A.; Dragoset, R. A.; Celotta, R. J. *Science* **1991**, *251*, 1206.

(29) Žutić, I.; Fabian, J.; Sarma, S. D. *Rev. Mod. Phys.* **2004**, *76*, 323.

(30) Donati, F.; Gragnaniello, L.; Cavallin, A.; Natterer, F. D.; Dubout, Q.; Pivetta, M.; Patthey, F.; Dreiser, J.; Piamonteze, C.; Rusponi, S.; Brune, H. *Phys. Rev. Lett.* **2014**, *113*, 177201.

Graphical TOC Entry

AFM delocalization manipulation of a Co atom on $p(2 \times 1)$Cu(110):O surface (left arrow) and its explanation by long-range Friedel forces exerted by the other Co adsorbates on the surface (right arrow).